Temperature and Hydrologic Cycle Constraints on Snowball Earth Environments

T. J. Mackey[1], A. B. Jost[1], J. R. Creveling[2], and K. D. Bergmann[1]

[1]Massachusetts Institute of Technology, Department of Earth, Atmospheric, and Planetary Sciences. [2]Oregon State University, College of Earth, Ocean, and Atmospheric Sciences.

Corresponding author: Tyler Mackey (tjmackey@mit.edu)

Key Points:

- Neoproterozoic strata preserve differences in clumped isotope records of glacial and non-glacial carbonates.
- Dolomites are partially altered in burial, but the glacial dolomite mean temperature is 16–36°C colder (95% CL) than pre-glacial dolomite.
- Mineral and reconstructed fluid $\delta^{18}O$ values are higher in glacial facies, suggesting continued hydrological cycling and evaporation.

Abstract

Pre- and syn-glacial low-latitude carbonate sediments of the Elbobreen Formation, NE Svalbard, preserve evidence for dramatic climate changes associated with Cryogenian glaciations (720–635 Ma). We combine carbonate stable ($\delta^{13}C$, $\delta^{18}O$) and clumped isotope (Δ_{47}) geochemistry with petrographic observations to assess the provenance of carbonate within glacial facies of the Petrovbreen Member and their environmental significance. Calcite Δ_{47} temperatures reflect solid-state reordering under burial temperatures, whereas dolomites record lower temperatures that vary with depositional facies. Pre-glacial dolomites have Δ_{47} temperatures from 48–73°C, with a reconstructed fluid $\delta^{18}O$ value of +0.6‰ (VSMOW) in the coldest sample. Glacial dolomites comprise: (1) detrital carbonate clasts similar to pre-glacial strata in stable isotope composition, Δ_{47} temperature, and petrographic textures; and (2) autochthonous dolomicrite and re-worked dolomicrite clasts with heavier $\delta^{18}O$ values and colder Δ_{47} temperatures of 19–44 °C. Measured dolomite temperatures likely include a component of diagenetic alteration that elevated the sample temperature above that imparted at deposition. The statistically significant difference in Δ_{47} temperatures between *in situ* precipitated matrix and re-worked detrital clasts in diamictite indicates that matrix samples preserve some component of carbonate that records early temperature differences either reflecting the primary sediments or early dolomitization and shallow lithification. The higher source fluid $\delta^{18}O$ values in glacial carbonates is consistent with an active hydrological cycle, either through local evaporation or growth of continental ice sheets sourced from evaporation of seawater. Continued hydrological cycling and 20–30 °C offsets in temperature between glacial and non-glacial conditions constrain carbonate depositional environments in this first Cryogenian glaciation.

Plain Language Summary

Glaciations known as Snowball Earth episodes took place in the late Precambrian (before 541 million years ago), and interpretations of their severity vary from more moderate conditions with liquid seawater at the equator to “hard” Snowballs with complete freezing of the ocean surface. It is important understand the severity of these glaciations as they are associated with many changes moving from the Precambrian dominated by microscopic life to the Phanerozoic (541 million years ago to present) with expansion of larger complex life. In this study, we analyzed carbonate sedimentary rocks from Svalbard that were originally deposited near the equator before and during one of these Snowball Earth events, reconstructing the temperature when these carbonates formed and the composition of their source waters. Carbonates maintain a record of significantly (20–30°C) lower temperatures in glacial deposits than in non-glacial deposits, but their composition also indicates that there was still evaporation taking place in the glacial environment. This evidence is more consistent with an active hydrological cycle at intervals during the Snowball Earth episode. Our results indicate that this approach to reconstructing ancient conditions may lead to a better understanding of how the climate operated in these pivotal periods of Earth history.

1 Introduction

Earth’s Phanerozoic climate was dominated by “greenhouse” conditions without polar ice, with brief forays into “icehouse” states similar to today (Brenchley et al., 1994; Montañez & Poulsen, 2013). Prior to the Phanerozoic Eon, peculiar, low-latitude, Neoproterozoic glacial

deposits provide evidence of a third, panglacial climate state colloquially referred to as a "Snowball Earth" (Harland et al., 1966; Hoffman et al., 1998; Kirschvink, 1992). Snowball Earth episodes are thought to represent a positive feedback between ice cover and albedo with expansion of sea ice to low latitudes, locking the planet into a perennially frozen state until volcanic outgassing and greenhouse warming overcomes albedo (Hoffman et al., 1998). Accordingly, the Snowball Earth hypothesis predicts that the onset and termination of low latitude glaciation should be globally synchronous (Kirschvink, 1992). Recent radiometric constraints have confirmed the synchronous initiation and termination of Neoproterozoic glaciations within the uncertainty of analyses (Macdonald et al., 2010; Rooney et al., 2015). This revised chronology indicates the earlier of the two Neoproterozoic Snowball glaciations lasted at least 57 Ma (Hoffman et al., 2017; Macdonald et al., 2010; Rooney et al., 2015), requiring climate dynamics distinct from subsequent Phanerozoic glaciations.

Conceptual and climate models of a persistently 'hard' snowball state—one with km-thick sea ice and initial mean annual equatorial temperatures <-20°C—predict a shutdown of the hydrologic cycle for millions of years (Abbot et al., 2013). Alternative climate models assert that such an extreme climate scenario is unnecessary to stabilize low latitude glaciations and that a panglacial state could have maintained a narrow strip of open water at low latitudes. These so-called "waterbelt" solutions avoid progression to a hard Snowball state due to negative feedbacks on ice advance, including a lower albedo of ablating sea ice and reduced cloud cover at low latitudes (Abbot et al., 2011). Differences in the hydrological cycling in these models make unique predictions for the evolution of seawater oxygen isotope composition during glacial intensification. Given the fractionation between liquid water and water vapor, evaporative export of marine water to continental ice sheets increased marine water oxygen isotope composition during Phanerozoic glacial-interglacial cycles (Shackleton, 1967), with marine $\delta^{18}O$ values approximately 3‰ higher in peak Pleistocene glaciation over estimated ice-free marine values of -1.2‰ (Cramer et al., 2011; Lea et al., 2000; Lear et al., 2000). This trend holds for the most recent glacial-interglacial transitions (Raymo et al., 2018), as well as earlier glacial episodes of the Late Paleozoic Ice Age (Grossman et al., 2008) and the end-Ordovician (Finnegan et al., 2011). Predictions for Snowball Earth marine $\delta^{18}O$ differ depending on the severity of the glaciation. A waterbelt solution would permit continued evaporation and precipitation from the marine reservoir, whereas a hard Snowball Earth would be marked by freeze-concentration during growth of the surrounding ice shell. Ice formation preferentially sequesters more ^{18}O-enriched water (Horita, 2008), leaving a depleted marine reservoir. Such fluid isotopic evolution commonly occurs via freeze-concentration in modern ice-covered environments in Antarctica, where $\delta^{18}O$ values for seawater-sourced saline lakes can be 5‰ lower than source water (Bird et al., 1991; Horita, 2008) and seawater-derived cryogenic brines reach $\delta^{18}O$ values of -8 to -11‰ after 1x freeze-concentration (Frank et al., 2010). Thus, reconstruction of marine fluid isotopic composition may provide an important constraint on the severity of glacial conditions in Snowball Earth episodes by assessing the relative contribution of evaporation and freeze concentration to marine fluid evolution.

1.1 Carbonate records of temperature and seawater composition

Carbonates associated with Cryogenian glaciations may be informative for climate models given predictions for seawater $\delta^{18}O$ values with different climate states. Marine fluid $\delta^{18}O$ is recorded in carbonates, but this fractionation is temperature- and mineral-dependent (Kim & O'Neil, 1997; Urey, 1948). For a specific mineralogy, temperature dependence complicates predictions of precipitation fluid conditions. Furthermore, carbonate $\delta^{18}O$ values are sensitive to alteration by diagenetic fluids, and primary $\delta^{18}O$ values can be diluted by incorporation of cements or overprinted by dissolution and reprecipitation (Dickson & Coleman, 1980; Huntington et al., 2011; Lohmann, 1988; Winkelstern & Lohmann, 2016). Interpretation of typical glacial climate from fluid $\delta^{18}O$ values is complicated, however, by significant uncertainty in the completeness of the stratigraphic section. Average sedimentation rates of Neoproterozoic glaciations are lower than for more recent glaciations, indicating that glacial strata integrate significant surfaces of erosion or non-deposition (Hoffman et al., 2017; Partin & Sadler, 2016). Interpretations of glacial severity from carbonate reconstructed fluid composition is accordingly limited to the environments where carbonates were deposited, potentially missing conditions typical of the Snowball Earth episodes. Nevertheless, any direct measurement of environmental conditions would provide important anchors for interpretation of climate dynamics within the Snowball Earth.

In order to constrain changes to seawater $\delta^{18}O$ values with glaciation, we have pursued carbonate clumped isotope thermometry of both pre- and syn-glacial carbonates of the Elbobreen Formation, NE Svalbard (Section 1.2). Carbonate clumped isotope thermometry is based on the temperature-dependent clumping of ^{13}C and ^{18}O into multiply substituted carbonate isotopologues (Eiler, 2007), which can be used to elucidate environments of carbonate precipitation and alteration. This thermometer constrains the temperature-dependent equilibrium water-carbonate ^{18}O fractionation for a given mineralogy (e.g. Kim & O'Neil, 1997), and can accordingly be used to calculate the $\delta^{18}O$ value for the fluid source of carbonates.

At any point during burial, processes including dissolution and reprecipitation or changes in mineralogy like dolomitization will move clumped isotope temperatures toward the local geothermal gradient (Bergmann et al., 2018; Ryb & Eiler, 2018; Winkelstern & Lohmann, 2016). Similarly, post-depositional cementation of primary grains also dilutes clumped isotope signatures with carbonate material that is equilibrated to burial temperatures (Mangenot et al., 2018). Thus, both the extent of alteration (itself a function of primary grain size, porosity and mineralogy; e.g. Bergmann et al., 2018; Staudigel & Swart, 2019) and the burial depth at which alteration takes place (Stolper et al., 2018) determine the magnitude of diagenetic change in clumped isotope temperature. Such processes can be variably fluid- or rock-buffered and affect carbonate $\delta^{18}O$ values differently. If carbonates experience fluid-buffered diagenesis, carbonates will approach mineral $\delta^{18}O$ values in equilibrium with the diagenetic fluids for that burial temperature (e.g. Bergmann et al., 2018; Huntington et al., 2011). In contrast, rock-buffered carbonates can show increased clumped isotope temperatures without a concomitant changes in mineral $\delta^{18}O$ values (e.g. Bergmann et al., 2018; Huntington et al., 2011; Staudigel & Swart, 2019).

Carbonate clumped isotope records can also be altered by solid state reordering. Solid state reordering is the re-equilibration of individual multiply substituted isotopologues within a carbonate mineral at elevated temperature (Henkes et al., 2014; Stolper & Eiler, 2015); this process leads to resetting of clumped isotope temperatures associated with carbonate precipitation to fully or partially reflect elevated burial temperatures. Models for this reordering explain experimental observations of reordering kinetics by 1) including diffusive propagation of defects (Henkes et al., 2014) or 2) a two-step reaction between adjacent carbonate molecules and successive diffusion through the carbonate crystal lattice (Stolper and Eiler, 2015). The kinetics of reordering over geologic timescales is temperature-dependent, and this relationship varies by carbonate mineralogy. Reordering experiments and supporting field studies of carbonate strata indicate that calcite reorders at temperatures above ~100°C over $10^{6} – 10^{8}$ years (Henkes et al., 2014), whereas dolomite begins to partially reorder above ~150°C over $>10^{7}$ years (Lloyd et al., 2018). Carbonates with burial temperatures below the threshold for solid state reordering could maintain primary and early diagenetic clumped isotope temperatures over 10^{8} years (Bergmann et al., 2018; Henkes et al., 2018).

1.2 Geologic Setting

The carbonate clumped isotope system is highly sensitive to post-depositional alteration, which indicates that low maximum burial temperatures are necessary to preserve climatically relevant information in deep time (e.g. Henkes et al., 2018). Thus, testing for Neoproterozoic climate transitions with clumped isotopes requires the coincidence of a well-defined stratigraphic record of carbonates across climate states and a shallow subsequent burial history. As presented below, the stratigraphy of NE Svalbard likely records one instance of such conditions. Strata consist of mixed siliciclastic and carbonate rocks originally deposited in a long-lived basin at low paleolatitudes (Fairchild et al., 1989; Hoffman et al., 2012; Maloof et al., 2006). Strata are made up of the Akademikerbreen, and Polarisbreen groups, and key sections are presently exposed along a 180 km belt across northeast Olav V Land, Ny Friesland, and west Nordaustlandet (Fairchild et al., 1989; Halverson et al., 2004; Harland et al., 1966) (Figure 1).

The onset of Cryogenian glaciation is preserved in the transition between the Russøya and Petrovbreen members of the Elbobreen Formation in the Polarisbreen Group. These members contain abundant carbonate and are the focus of this study. Regionally, the Russøya Member begins with a transgression over peritidal facies of the Dartboard Dolomite Member in the Backlundtoppen Formation of the Akademikerbreen Group. This transgression reflects the start of two marine transgressive-regressive sequences in the Russøya Member (T-R7 and 8 of Halverson et al., 2004; 2018). Lower transgressive Russøya Member strata are composed of calcite, but transition to dolomite up section (Halverson et al., 2004; 2018). The overlying Petrovbreen Member varies in thickness across NE Svalbard, with the thickest sections exceeding 50 m in Ny Friesland. These strata include dolomitic rhythmite, wackestone containing outsized clasts interpreted as glacial dropstones, and diamictite with siliciclastic or dolomicrite matrix (Fairchild et al., 1989; Halverson et al., 2004). Facies are interpreted as marine or glaciolacustrine depositional environments and vary from subglacial and grounding line facies to more distal facies with ice-rafting (Fairchild et al., 1989; Hambrey, 1982; Hoffman et al., 2012).

Dolomicrites are only present intermittently in the Petrovbreen Member (Figure 1) and are not a common facies in other correlated glacial sections (Spence et al., 2016; Spencer, 1971). As such, it is possible that these carbonates do not capture the peak intensity of a 'hard' snowball, and may instead reflect conditions particular to this glaciated carbonate platform with local increases in alkalinity from glacial processing of detrital carbonate (c.f. Fairchild et al., 2004). Stratigraphic relationships suggest that Petrovbreen Member dolomicrites do not represent deposition within the final deglaciation, as the diamictite successions in Svalbard are cross-cut by sediment-filled wedges interpreted as periglacial exposure surfaces (Fairchild et al., 1989). Such exposure surfaces require progressive fall in base level, possibly indicative of glacial intensification subsequent to emplacement of strata hosting glacial carbonates.

The Petrovbreen Member lacks direct geochronological constraints but has been correlated to the first glacial episode of the Cryogenian (Halverson et al., 2018; Hoffman et al., 2012), colloquially termed the Sturtian glaciation. Chemical evidence to support the Sturtian age assignment comes from the similarity of the upper Russøya Member $^{87}Sr/^{86}Sr$ values to Tonian values (Hoffman et al., 2012) and corresponding stratigraphic association with a negative carbon isotope excursion identified as the Islay anomaly (Halverson et al., 2018; Hoffman et al., 2012). If the Sturtian correlation is valid, the upper Russøya Member was deposited between ~740–735 Ma (Halverson et al., 2018; MacLennan et al., 2018; but see Fairchild et al., 2017 for discussion of ambiguity in pre-Sturtian carbon isotope stratigraphy). Biostratigraphy further supports a pre-Sturtian correlation for the Russøya Member. Vase-shaped microfossils (VSM) are present in the Russøya Member in NE Svalbard (Knoll & Calder, 1983), similar to other pre-Sturtian strata where geochronology is well-constrained (Cohen & Riedman, 2018). Together, chemo- and biostratigraphy highlight the potential for these carbonates to record meaningful information about the onset of glacial conditions in the Cryogenian.

The burial history of Ny Friesland is poorly constrained, but regionally Ordovician strata of the Oslobreen Group disconformably overlying Neoproterozoic strata have organic preservation inconsistent with deep burial. In NE Ny Friesland, conodont color alteration indices are 1 (Bergström, 1980), which indicates burial temperatures <80°C (Epstein et al., 1977). These strata also contain intact biomarkers consistent with mid-oil window thermal maturity (Lee et al., 2019). Despite such evidence for low thermal alteration, Ny Friesland was affected by the Caledonian Orogeny (Gasser, 2014 and references therein); Neoproterozoic and overlying Cambro-Ordovician strata are steeply dipping and faulted (Fairchild & Hambrey, 1984; Hoffman et al., 2012). Across Ny Friesland, thermal modeling from apatite fission track analysis indicates that there is a strong local fault control on exhumation history, with total exhumation of Caledonian granites estimated at 4-6 km on some fault blocks since 180–80 Ma (N. Dörr et al., 2012; Nina Dörr et al., 2019). Such maximum burial exceeds the constraints from local organic preservation (Bergström, 1980; Lee et al., 2019), highlighting the potential for significant heterogeneity in maximum burial among fault blocks.

1.3 Neoproterozoic clumped isotope thermometry in Svalbard

Here we present carbonate clumped isotope data for carbonate-rich pre- and syn-glacial strata associated with the first Cryogenian glaciation cropping out in the Elbobreen Formation, NE Svalbard (Fairchild et al., 1989; Halverson et al., 2004; Harland et al., 1966; Figure 1). Given the sensitivity of the carbonate clumped isotope system to reordering with burial and the local diagenetic environment and solid state reordering during burial (Section 1.1), any attempt to assess changes in climate using this thermometer must first characterize evidence for solid state reordering as well as both diagenetic alteration and timing of crystallization events. In order to avoid confounding lateral heterogeneity in maximum burial throughout Ny Friesland, we have restricted this study to the Ny Friesland Dracoisen nunatak. Carbonates include both calcites and early fabric-retentive dolomites, and because of the different susceptibility of these minerals to solid state reordering (Henkes et al., 2014; Stolper & Eiler, 2015), the divergence of clumped isotope temperatures can be used to estimate of maximum burial temperatures and to constrain the extent of solid state reordering in strata at the Dracoisen nunatak. With the understood complications of burial diagenesis and solid state reordering, the juxtaposition of carbonates across contrasting climate states available at the Dracoisen nunatak provides an ideal test for the preservation of differences in carbonate clumped isotope temperatures and reconstructed fluid $\delta^{18}O$ values set by climate extremes of the Cryogenian.

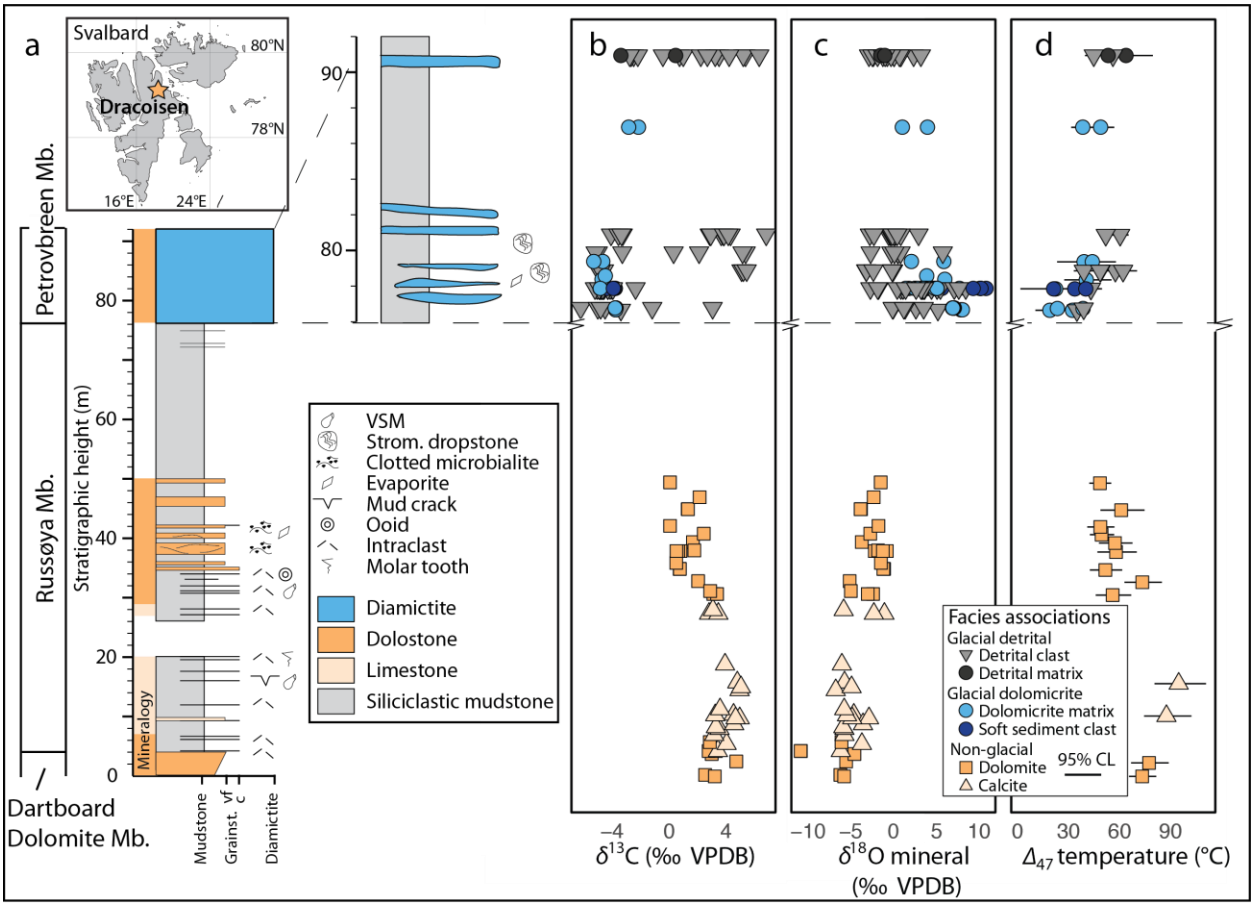

Figure 1: Stratigraphy of the latest Tonian (Dartboard Dolomite and Russøya members) and earliest Cryogenian (Petrovbreen Member) at the Dracoisen Nunatak, NE Svalbard. a) Stratigraphic column highlighting transitions among the dominant carbonate mineralogies. The scale of the Petrovbreen Member is extended to display diamictite distribution. b) Composite of $\delta^{13}C$ values and c) Mineral $\delta^{18}O$ value through stratigraphic section. d) Clumped-isotope temperatures and 95% CL error.

2 Materials and Methods

2.1 Field localities and sampling

Carbonates from the Dartboard Dolomite Member of the Backlundtoppen Formation, Akademikerbreen Group and overlying Russøya and Petrovbreen members of the Elbobreen Formation, Polarisbreen Group were collected in stratigraphic context on the Dracoisen nunatak, NE Ny Friesland, Svalbard on a field campaign in 2014 (GPS 79.204931, 18.345240). Carbonate samples were collected at approximately 1 m intervals where present (Table S1). This suite was supplemented with four samples of the Petrovbreen Member previously collected by Ian Fairchild (University of Birmingham) from the Dracoisen nunatak. Due to lateral heterogeneity in Petrovbreen Member stratigraphy these samples are integrated into the section detailed in this study using their stratigraphic height relative to marker beds. The section targeted for this study was previously mapped (e.g. Fairchild et al., 1989; Halverson et al., 2004). Our additional observations of stratigraphic relationships and facies in these strata are placed within this framework for correlation.

2.2 Petrography and mineral identification

Carbonate samples were cut to remove weathered surfaces prior to petrographic and geochemical analysis. All samples collected for clumped isotope analysis (n=24) were slabbed, polished and scanned (Figure S1) to aid in the identification of target carbonate textures to drill for subsequent subsampling and analysis (n=41). Of the 24 slabbed samples, 20 were thin sectioned for petrographic characterization of target textures. We further analyzed 17 drill sites for mean crystal size using 25 representative crystals from each sampled carbonate texture. Measurements were made using ImageJ software from thin section photomicrographs following the method of Bergmann et al., 2018a (Table S1).

Sample mineralogy was determined based on X-ray diffraction (XRD) or dilute acid reaction (Table S1). For XRD, splits of powdered samples were analyzed on a PANalytical X'Pert PRO x-ray powder diffractometer (XRPD) housed in the MIT Center for Materials Science and Engineering (MIT-CMSE) to quantify the abundance of calcite, dolomite, and other minerals. For each sample, approximately 500 µg of powder was analyzed for two hours from 5° to 90° on a spinning stage at a fixed irradiated length**.** We describe carbonate microfacies after Fairchild et al. (1989) and adopt the term (dolo)micrite in reference to carbonate crystals less than 10 µm in diameter, (dolo)microspar for crystals between 10 and 50 µm in diameter, and spar for mean crystal diameter > 50 µm.

2.3 Isotopic analysis

Carbonate $\delta^{13}C$, $\delta^{18}O$, and clumped isotopic (Δ_{47}) analyses were performed at MIT on a Nu Perspective isotope ratio mass spectrometer coupled to a Nu Carb automated carbonate sampler. Samples of specific carbonate textures were drilled using carbide bits at low speed to produce homogeneous powders for isotopic analyses. Clumped isotope analysis had different methods from samples solely analyzed for bulk $\delta^{13}C$ and $\delta^{18}O$; these methods are presented separately below.

291

292 2.3.1 Carbonate clumped isotope (Δ_{47}) analysis

293 For Δ_{47} measurements, we analyzed ~450 µg of carbonate powder drilled from polished
294 sample slabs; weights for samples with lower weight percent carbonate as determined by CO_2
295 yield were increased to match the carbonate mass of the pure standards and ranged from ~450 to
296 900 µg. Carbonates were digested in sample vials with 150 µL H_3PO_4 (1.94–1.95 g/cm^3); see
297 supporting information for detailed description of clumped isotope analytical methods (Text S1).
298 Clumped isotope data were processed using Easotope software (John and Bowen, 2016), ^{17}O
299 corrections after Schauer et al. (2016) and Daëron et al. (2016). Raw $\delta^{13}C$, $\delta^{18}O$ and clumped
300 isotopic (Δ_{47}) measurements were transferred to VPDB and Carbon Dioxide Equilibrium Scale
301 (CDES) (Dennis et al., 2011), respectively, using four ETH carbonate standards (after
302 Bernasconi, et al., 2018). Calcite and dolomite Δ_{47} values were further corrected with a 70°C
303 acid fractionation factor of 0.062 (Defliese et al., 2015; Müller et al., 2017). All samples passed
304 screening for contamination using Δ_{48} values; all samples had Δ_{48} values with a lower absolute
305 value than the cutoff of <0.5‰. Samples were only incorporated into this study where ≥3
306 replicates passed all screening tests (Text S2).

307

308 Analyses were carried out over the course of 1.5 years (6/2017–11/2018), during which
309 time instrument upgrades and repairs led to changes in precision of analyses. In the course of this
310 study, long term standard deviation of reference materials (1 SD) varied from 0.02 to 0.04‰,
311 0.02 to 0.07‰, and 0.06 to 0.20‰ for Δ_{47}, $\delta^{13}C$, and $\delta^{18}O$ values respectively. Raw data for all
312 standards and sample replicates are available in supporting information and are posted at
313 EarthChem (Table S2 to be submitted to EarthChem on manuscript acceptance).

314

315 We calculated precipitation temperature following the Δ_{47}–temperature relationship of
316 Bernasconi et al. (2018). Additional discussion of dolomite temperature calibrations are
317 presented in the supporting information (Text S3). Precipitating fluid $\delta^{18}O$ values were
318 calculated from mineral $\delta^{18}O$ values and Δ_{47} temperatures, assuming equilibrium fractionation
319 between fluid and mineral $\delta^{18}O$ following the temperature–fractionation relationship of Kim and
320 O'Neil (1997) for calcite and Horita (2014) for dolomite. Error for clumped isotope temperatures
321 are presented as 95% confidence levels from sample replicates (Fernandez et al., 2017) for
322 conservative estimates of error in reconstruction, whereas populations of data points from
323 different samples are discussed with reference to one standard deviation to highlight the
324 distribution of temperatures in the population.

325

326 2.3.1 Carbonate $\delta^{13}C$ and $\delta^{18}O$ microvolume analysis

327 Samples of ~100µg carbonate were analyzed for $\delta^{13}C$ and $\delta^{18}O$. Samples spanned the
328 Dracoisen stratigraphy at the m-scale resolution of sampling, and select carbonate textures
329 analyzed for Δ_{47} were drilled at the mm-scale to assess compositional heterogeneity (Figure S2.
330 Microvolume analysis of drilled samples consisted of digestion in H_3PO_4 (1.91–1.92 g/cm^3) at
331 70°C, followed by cryogenic purification. Sample beam analysis consisted of 6 cycles of 20s
332 integration. Results were processed using Easotope software (John & Bowen, 2016) translated to

the VPDB reference frame using ETH and in-house standard materials. Long term standard deviation of reference materials (1 SD) throughout the course of analysis (01/2018–09/2018) varied from 0.04–0.09‰ and 0.07–0.17‰ for $\delta^{13}C$ and $\delta^{18}O$, respectively, in individual correction intervals.

3 Results

3.1 Carbonate petrography

The stratigraphic distribution of facies documented in our study is broadly consistent with those of previous authors (Fairchild et al., 1989; Halverson et al., 2004, 2018); we build on these facies associations and our petrographic observations to group the isotope analyses in Dracoisen section pre- and syn-glacial carbonates (Figure 2).

The lowest stratigraphic section examined in this study is the upper Dartboard Dolomite Member. These strata are composed of stylotized dolomicrospar (mean crystal sizes 14–23 μm), with local sheet crack-filling dolospar. The Dartboard Dolomite Member transitions upwards to limestones of the lower Russøya Member, which are composed of microspar and intraclastic grainstone. Rare mud cracks and molar tooth textures are also present. Up section, Russøya Member carbonates change to dolomite composed of stromatolites with a clotted microtexture, intraclastic and rare oolitic grainstones, and contain rare evaporite pseudomorphs. The crystal size of Russøya Member dolomites varies with texture. The finest dolomicrites (<5 μm) are present in stromatolite clots, whereas laminated dolomites are typically micritic to microsparitic (mean crystal sizes 17±8 μm, 1 sd), including laminae intercalated on the mm-scale with the finest dolomitic clots.

The overlying Petrovbreen Member carbonates analyzed here are dolomitic, with varying contribution of chert clasts, silicate minerals, and subsidiary siliciclastic grains. Siliciclastic grains include rare grain aggregates, and we have interpreted these aggregates as till pellets (Figure S3), consistent with the prevailing interpretation of a glaciomarine or glaciolacustrine depositional environment (Fairchild et al., 1989; Halverson et al., 2018; Hambrey, 1982). Dolomites consist of three components defined by their crystal/grain size, texture, and relationship to surrounding sediments. (1) Dolomicrite (mean crystal size <5 μm) is present in the Petrovbreen Member as homogeneous beds, interlaminated with coarser carbonate grains in varves, within ductily deformed soft sediment clasts, or as a matrix between larger clasts. Dolomicrite matrix is present in both stratified diamictites and matrix-supported diamictite samples without lamination or clast sorting. Dolomicrite purity varies in samples analyzed by XRD, with compositions ranging from >70% dolomite to a subsidiary component mixed with more abundant quartz as well as other silicate minerals (Table S3). (2) >1 mm angular to well-rounded clasts with constituent carbonate fabrics that are stromatolitic, clotted, fenestral, laminated, intraclastic, and dolomicritic. These larger angular to well-rounded clasts are hereafter referred to as detrital clasts. Detrital clasts have a range of mean crystal sizes, with stromatolitic, clotted, fenestral, laminated, and intraclastic carbonate fabrics having mean crystal sizes ≥10 μm in contrast to the finer dolomicrites. Rare detrital clasts from the stratified diamictite have circumgranular sparry crusts up to 100 μm thick (Figure S3) (3) Carbonate clasts <1 mm form

376 the matrix between the larger detrital clasts. Petrovbreen Member dolomite components vary
377 stratigraphically. Dolomicrite is most abundant in the lowermost 2 m of the Petrovbreen Member
378 below a brecciated surface (Fairchild, pers. comm.) containing abundant pseudomorphs
379 consistent with sulfate minerals. Additional dolomicrite is present above this surface as
380 homogeneous dolomicrite, diamictite matrix and fine rhythmite laminae, but the majority of
381 carbonates consist of detrital clasts in diamictite beds or dropstones in siliciclastic mudstone
382 (Figure 1A).

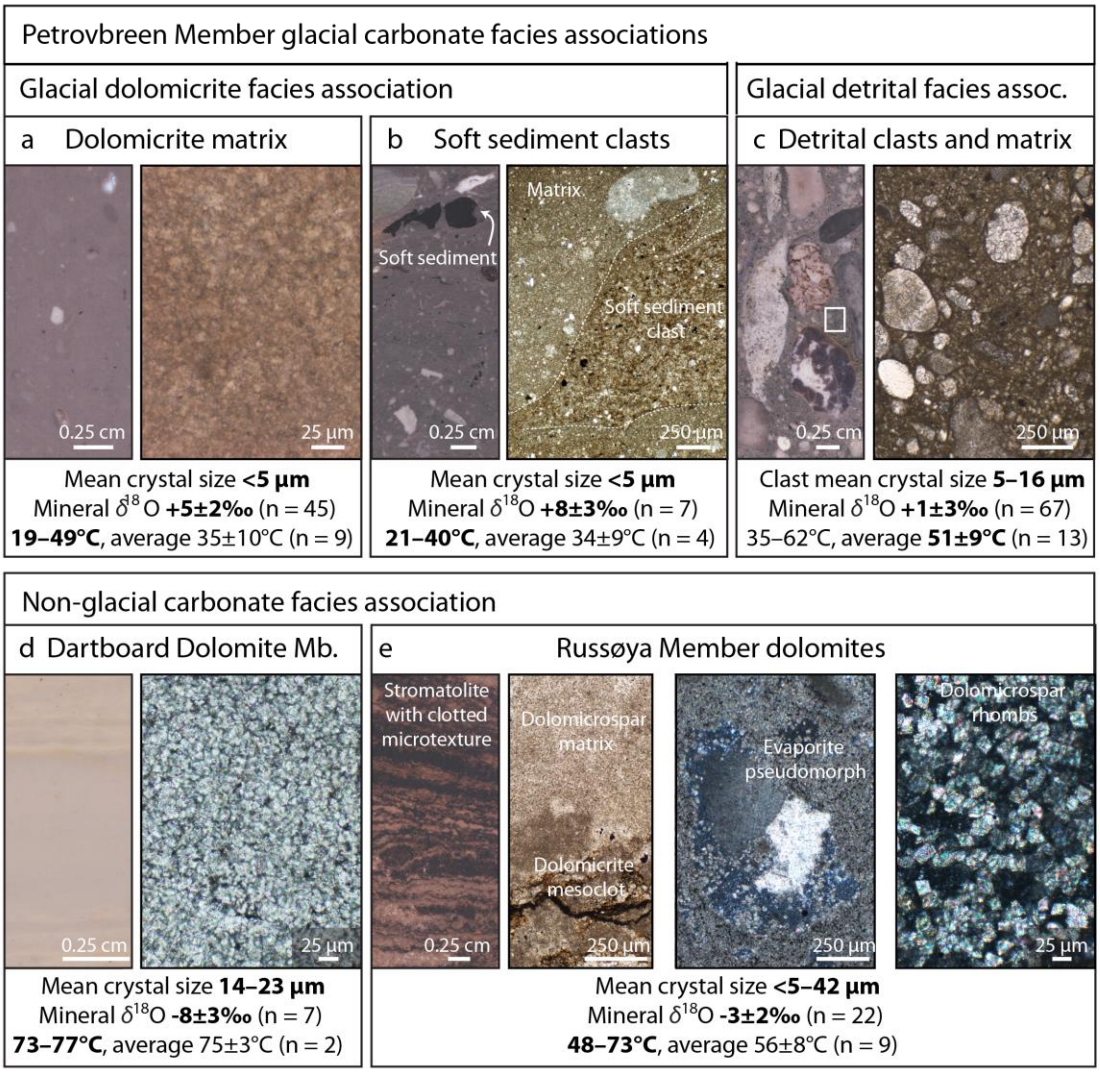

Figure 2: Petrographic textures of the Dracoisen section dolomites; where images are paired, left is a scanned polished sample and right is thin section photomicrograph. a–c) Glacial carbonates of the Petrovbreen Member consisting of a) homogeneous dolomicrite matrix, b) discrete soft sediment clasts in diamictite, c) detrital clasts and matrix consisting of <1 mm detrital clasts. d and e) non-glacial carbonates of the d) peritidal Dartboard Dolomite Member of the Akademikerbreen Formation and e) overlying Elbobreen Formation Russøya Member. Russøya Member dolomite facies pictured here include stromatolites with a clotted microtexture, evaporite pseudomorphs partially replaced by dolomite and silica (here cross-polarized to highlight twinning after gypsum), and homogeneous dolomicrospar rhombs in wedged thin section. Mean crystal sizes indicate range in mean sizes for analyzed samples, and isotope data present the mean mineral $\delta^{18}O$ values and clumped-isotope temperatures ±1 standard deviation to describe the population analyzed, and the range of mean clumped isotope temperatures.

383

Together, the Dracoisen stratigraphy comprises three broad facies associations. The Dartboard Dolomite and Russøya members make up (1) the non-glacial facies association, which are possible source strata for subsequent glacial erosion and redeposition. The Petrovbreen Member carbonates make up two facies associations based on petrographic texture: (2) the glacial dolomicrite facies association includes homogeneous dolomicrite, dolomicrite matrix, soft sediment clasts, and fine varve laminae; (3) the glacial detrital facies association includes both the larger detrital dolomite clasts and matrix material composed of recognizable finer <1 mm dolomite clasts. The geochemistry of these three facies associations are detailed in the following sections.

3.2 Non-glacial facies association isotope analyses

Carbonate $\delta^{13}C$ and $\delta^{18}O$ isotopic composition vary stratigraphically (Figure 1B and C). $\delta^{13}C$ values greater than +2‰ characterize the Dartboard Dolomite and lowermost Russøya members. $\delta^{13}C$ values peak at +5.1‰ in the calcite strata of the lower Russøya Member and decrease to +0.5‰ over 20 m up section through the transition to dolomite. $\delta^{13}C$ values in the subsequent dolomite beds remain between +0.1‰ and +2.4‰ through the transition to shale in the upper Russøya Member. Mean mineral $\delta^{18}O$ values increase through the Dartboard Dolomite and Russøya members, from -7±2‰ (1 sd) in the Dartboard Dolomite Member, to -5±2‰ (1 sd) in the lower Russøya Member calcites and -2±1‰ (1 sd) in the overlying Russøya Member dolomites (Figures 1 and 3, Table S1).

Reconstructed clumped isotope temperatures through the non-glacial facies also show distinct trends across lithology and depositional environment (Figure 1D). Where calcite beds and veins co-occur in the Russøya Member, these facies record warmer temperatures than dolomite. Calcite samples from bedded strata and cross-cutting veins record mean temperatures of 92±5°C (n=2, 1 sd) and 122±4°C (95% CL), respectively (Figure 3A). Dolomites in non-glacial strata preserve a range of clumped isotope temperatures from 48 to 77°C (Figure 1D, Table S1). Peritidal facies of the Dartboard Dolomite member record higher temperatures (75±3°C, n=2, 1 sd) compared to the immediately overlying Russøya Member dolomites (56±8°C, n=9, 1 sd) (Figure 1D, Table S1).

Reconstructed fluid compositions calculated from mineral $\delta^{18}O$ and clumped isotope temperatures also vary by facies and mineralogy across the non-glacial stratigraphy (Figure 3A). Samples of the Dartboard Dolomite member have reconstructed fluid compositions of +1.9±0.9‰ (1 sd, n=2, Table S1). Reconstructed fluid composition of the Russøya Member varies with mineralogy (Figure 4A): calcite reconstructed fluid $\delta^{18}O$ values are +8.3±0.1‰ (1 sd, n=2), whereas Russøya Member dolomites have reconstructed fluid $\delta^{18}O$ values from +0.7 to +3.0‰ (+1.9±0.8‰, 1 sd n=9, Table S1).

3.3 Glacial dolomicrite facies isotope analyses

Relative to the underlying non-glacial stratigraphy, dolomicrite of the Petrovbreen Member has negative $\delta^{13}C$ (-4.4±0.6‰, 1 sd n=45) and positive $\delta^{18}O$ values (+5±2‰ 1 sd n=45). The fine-scale isotopic variability of this dolomicrite differs between matrix-supported and stratified diamictite samples, however. The dolomicrite of matrix supported diamictite is isotopically homogeneous where subsampled for microvolume analyses, with $\delta^{13}C$ and $\delta^{18}O$ values within analytical uncertainty (-3.75±0.02‰ and +6.98±0.08‰, respectively, 1 sd n=8). Where dolomicrite forms the matrix of stratified diamictites 1 m above the matrix supported diamictite, $\delta^{18}O$ values vary at the mm-scale through stratified layers, from +1.4 to +7.7‰ (mean +4.1±1.2‰, 1 sd n=29). $\delta^{13}C$ values are more consistent, with a mean of -4.7±0.1‰ (1 sd n=29). Within the same sample, soft sediment clasts have similar $\delta^{13}C$ values as the mean matrix dolomicrite (-3.9±0.2‰ 1 sd n=6), but with higher $\delta^{18}O$ values (+9.4±1.8‰ 1 sd n=6; Figure S2).

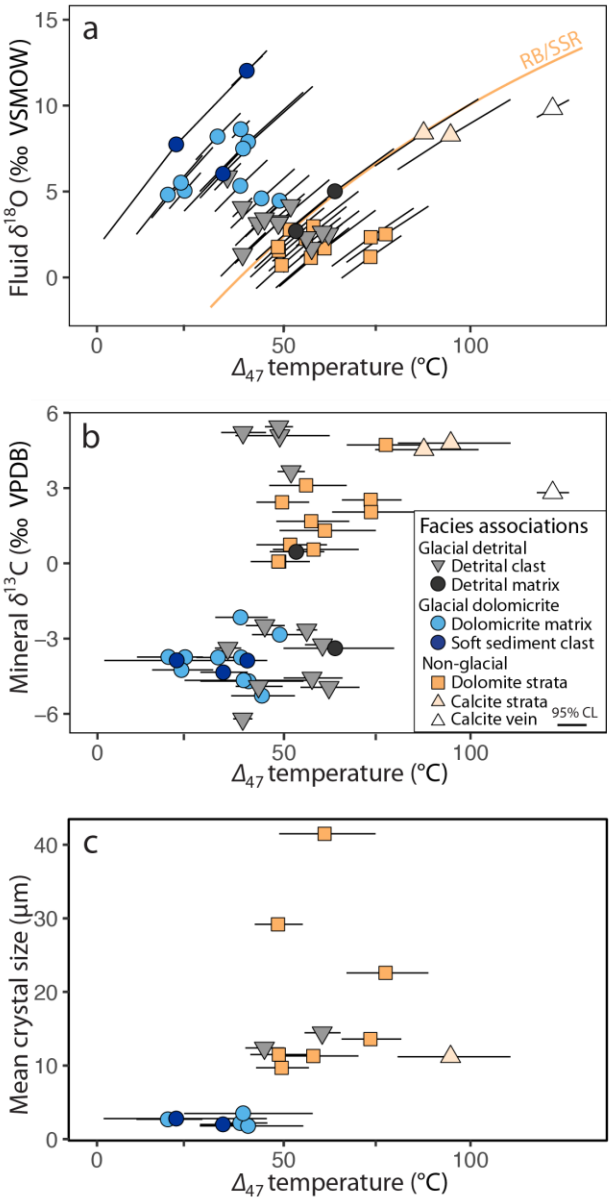

Figure 3: Summary of standard and clumped isotope values with petrographic observation. a) Measured clumped-isotope temperature for carbonate samples versus the reconstructed fluid $\delta^{18}O$ values. 95% CL error bars are diagonal due dependence of reconstructed fluid $\delta^{18}O$ values on measurement temperature. RB/SSR line denotes reconstructed fluid composition for dolomites (Horita, 2014) under purely rock-buffered alteration or solid state reordering, given a starting fluid composition of -1.2‰. b) Measured clumped isotope temperature versus mineral $\delta^{13}C$. c) Mean crystal size varies with clumped isotope temperatures. Mean crystal size of diamictite clasts is consistent with the source stratigraphy inferred from reconstructed $\delta^{18}O$ fluid values and clumped-isotope temperatures. Calcite versus dolomite mineralogy does not appear to correspond to a significant difference in mean crystal size, despite elevated calcite temperatures interpreted as evidence of solid-state reordering. Crystal sizes <5 µm are approximate due to thickness of petrographic thin sections.

Matrix dolomicrite clumped isotope temperatures range from 19 to 49°C, with mean temperatures 35±10°C (n=10, 1 sd; Figures 1D; 3A). Within a hand sample, dolomicrite with coarser crystal sizes associated with local alteration (Fairchild, 1983) has warmer clumped isotope temperatures than in adjacent finer dolomicrite (49 +8/-7°C versus 38±7°C, 95% CL; Table S1). Clasts featuring soft sediment deformation also have clumped isotope temperatures similar to the dolomicrite matrix, ranging from 21 to 40°C (31±10°C, n=3, 1 sd, Figure 1D; Table S1). The reconstructed fluid $\delta^{18}O$ values for the lowest temperature (<25°C, n=4) dolomicrite samples and soft sediment clasts range from +4.8 to +7.7‰ (Figure 3A).

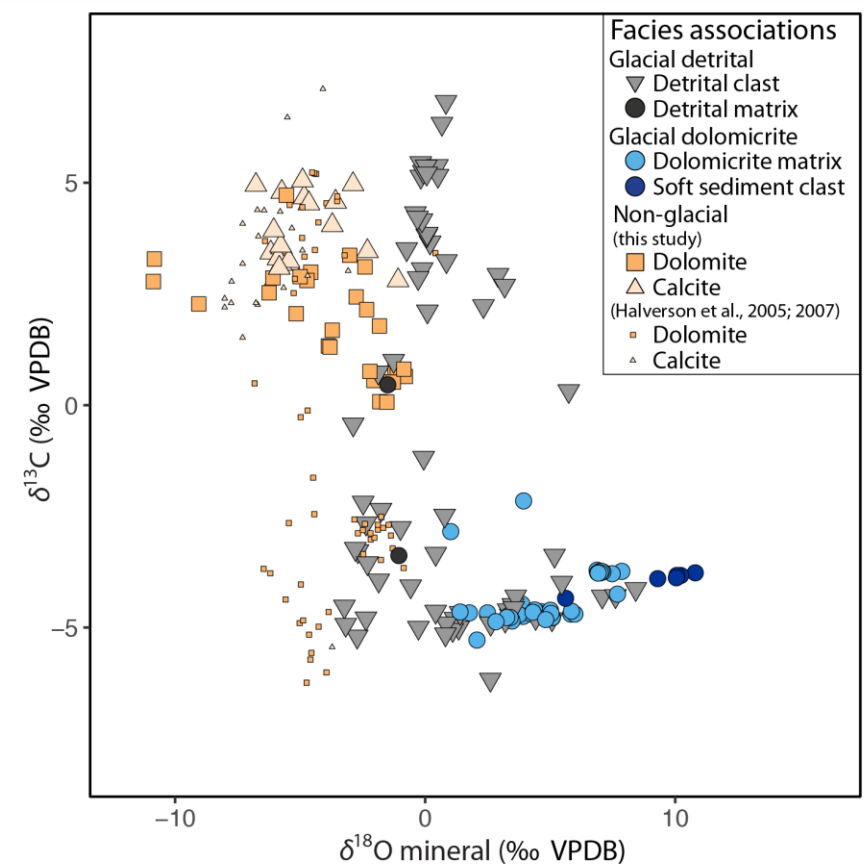

Figure 4: Cross plot of carbonate $\delta^{13}C$ and $\delta^{18}O$ values from the Tonian–Cryogenian in NE Svalbard. Pre-glacial carbonates from Halverson et al. (2005; 2007) sample the Russøya Member regionally. $\delta^{13}C$ and $\delta^{18}O$ values for the underlying Akademikerbreen Formation are presented in Figure S4. Glacial Petrovbreen Member carbonates sampled here are exclusively dolomitic. Diamictite clasts span the full range of $\delta^{13}C$ values in the underlying stratigraphy, but are generally more enriched in ^{18}O. Heterogeneous Petrovbreen Member carbonate isotopic values are consistent with multiple carbonate sources, here interpreted as a detrital carbonate source with comparable $\delta^{18}O$ values to underlying non-glacial stratigraphy and a glacial source with higher $\delta^{18}O$ values.

3.4 Glacial detrital facies association isotope analyses

Clumped isotope temperatures and $\delta^{13}C$ and $\delta^{18}O$ values of detrital clasts span much of the range of both the non-glacial and glacial dolomicrite facies associations (Δ_{47} 35–62°C, n=12; $\delta^{13}C$ -5.2 to +6.8‰, and $\delta^{18}O$ -3.2 to +8.4‰, n=68; Figures 1, 3 and 4). Comparable clumped isotope temperatures and $\delta^{18}O$ values between detrital clasts and surrounding stratigraphy correspond to a similar range of reconstructed fluid $\delta^{18}O$ values (+1.3 to +5.9‰; Figure 3A). Where the diamictite matrix is composed of fine detrital clasts, the $\delta^{13}C$ and $\delta^{18}O$ values are comparable to the surrounding detrital clasts (Figure 4). These samples also have clumped isotope temperatures similar to the warmest clasts (59±7°C, n=2, 1 sd; Figure 3A, B).

Clumped isotope temperatures and mineral $\delta^{18}O$ values also correlate with carbonate texture. Detrital clasts that resemble non-glacial strata with stromatolitic, clotted, or fenestral textures share similar isotopic compositions with them: $\delta^{18}O$ values span -3.2 to +0.8‰ for seven such clasts, and their clumped isotope temperatures range from 39 to 62°C (Table S1).

4 Discussion

Tonian and Cryogenian carbonates from the Dracoisen section preserve aspects of the timing and style of their diagenesis through petrographic textures and isotopic compositions. In the following discussion, we explore the source and preservation of Petrovbreen Member glacial carbonates to interpret clumped isotope record at the onset of the Cryogenian.

4.1 Records of calcite reordering with deep burial

Isotopic composition varies systematically with carbonate lithofacies, petrographic relationships and, where co-occurring in the non-glacial facies association, mineralogy. Within the Russøya Member, clumped isotope temperatures and reconstructed fluid compositions are higher in calcite than dolomite (Figure 3). The preferential solid state reordering of calcite at lower temperatures than dolomite explains this mineral-dependent relationship (Lloyd et al., 2018; Passey & Henkes, 2012; Stolper & Eiler, 2015). Clumped isotope temperatures from carbonate strata and reconstructed fluid $\delta^{18}O$ values follow trajectories consistent with low water-rock alteration or solid state reordering from an original marine source (Figure 3). In addition to these alteration trajectories, comparison of calcite strata temperatures (92±5°C; n=2, 1 sd) and cross-cutting calcite vein cement (122±4°C; 95% CL) provides a minimum burial temperature estimate. Based on laboratory reordering experiments and field observations, over 100 Ma calcite begins to be impacted at ~100°C, and calcites are 99% reordered at 144°C (values for brachipod calcite, Passey and Henkes, 2012; Henkes et al., 2014). Thus, although calcites have likely been impacted by solid state reordering, preservation of temperature differences between calcite strata and cross-cutting vein calcite indicates only partial solid state reordering of the calcites. Taken together, these results indicate that calcite clumped isotope temperatures represent a signature of deep burial rather than depositional or early diagenetic conditions. Burial temperatures are not likely to have significantly exceeded that recorded in calcite veins, however, as the kinetics of reordering would lead to rapid equilibration of calcite to higher temperatures.

Burial temperatures reflected by calcite reordering is within the upper bounds predicted for preservation of dolomite clumped isotope temperatures (Lloyd et al., 2018), consistent with their lower clumped isotope temperatures in the Dracoisen strata. Non-glacial dolomite temperatures do exceed expectations for reasonable surface conditions (48–77°C), indicating that they contain a signature of burial diagenesis. In the following discussion, we assess the relationships among petrographic textures, bulk isotope compositions, and clumped isotope temperatures to characterize the effect of diagenetic alteration on original climate signatures.

4.2 Dolomite sources across facies and timing of precipitation

The dolomite facies associations defined in this study have distinct petrographic textures, standard carbonate isotope compositions and clumped isotope temperatures. Carbonates from the non-glacial and glacial dolomicrite facies associations cluster separately by these metrics, but the detrital facies association contains clasts that display similar petrographic texture, crystal size distribution, and isotopic composition with both of the other facies associations (Figures 3 and 4). Taken together the wide range of $\delta^{13}C$ values found in Russøya Member carbonates regionally (>+7 to <-4.5‰; Hoffman et al., 2012; Halverson et al., 2018) is consistent with the composition of carbonate clasts found in the Petrovbreen Member. Indeed, petrographically distinctive clasts, such as stromatolite morphologies like those found in the nadir of the purported Islay negative carbon isotope excursion (Hoffman et al., 2012; Table S1), have $\delta^{13}C$ values (<-4.5‰), low mineral $\delta^{18}O$ values, and clumped isotope temperatures consistent with the underlying interpreted source stratigraphy. Temperatures of ≤25°C (n=4) are restricted to Petrovbreen Member samples of matrix dolomicrite and clasts featuring soft sediment deformation (Figures 1D and 4).

Temperature, $\delta^{18}O$ and $\delta^{13}C$ heterogeneity is maintained on the scale of clasts and matrix material (Figure S1), indicating that dolomites represent distinct populations with different depositional or early diagenetic histories. Temperature differences between the clasts and matrix of Petrovbreen Member diamictite require that dolomitization of clasts predated redeposition in the diamictite; dolomitization would affect clumped isotope composition of carbonates, even under low water-rock conditions that could have preserved primary carbonate $\delta^{18}O$ values (e.g. Ferry et al., 2011). Petrographic textures support this early dolomite source, including both dolomite crystal size distributions and accessory mineral assemblages. For example, heterogeneous petrographic textures, mineral $\delta^{18}O$ values, and clumped isotope temperatures are most consistent with a depositional or early diagenetic source of dolomite within pre-glacial stratigraphy, prior to erosion and re-deposition as clasts in the overlying diamictite. In addition to these distinct pre-glacial clasts in the diamictite, some stratified diamictite samples also contain clasts compositionally and texturally similar to the matrix dolomicrite. This relationship is consistent with local reworking of dolomicrite material in the depositional environment prior to sedimentation of the stratified diamictite.

The high $\delta^{18}O$ values of the Petrovbreen Member dolomicrite are also distinct from other dolomites in this stratigraphic section. The fine size of dolomicrite crystals has previously been interpreted as evidence for deposition as carbonate rock flour (Fairchild, 1983), however the coincidence of high $\delta^{18}O$ and low $\delta^{13}C$ mineral values in the diamictite matrix differ from the regional composition of dolomitic strata that could serve as the rock flour protolith (Halverson et al., 2018; Figure 4S). The isotopic composition of fine-grained glacial strata and soft sediment clasts instead fall on a mixing line away from underlying strata and recognizable exogenous carbonate clasts (Figure 4). The glacial dolomicrite of the Petrovbreen Member is also geochemically distinct from overlying cap dolostone and dolomitic silt-shale of the MacDonaldryggen Member, which have lower $\delta^{18}O$ values than the glacial dolomicrite (-8.6 – +0.6‰ with a mean of -3.7‰; Fairchild et al., 2016; Figure S4). Interglacial dolomite petrography indicates that MacDonaldryggen Member dolomite precipitation predated

compaction; pore-filling calcite interpreted as later burial cements are also associated with more negative $\delta^{18}O$ values around -9‰ (Fairchild et al., 2016).

Clumped isotope temperatures of Petrovbreen Member dolomicrite further constrain the source and timing of dolomite formation. Temperatures as low as 19 +9/-8°C (95% CL) are inconsistent with precipitation in deep burial conditions during nonglacial periods, particularly given low reconstructed paleolatitudes (Maloof et al., 2006). Thus, the composition of the glacial dolomicrite facies association is consistent with a distinct carbonate precipitating at low temperatures from a fluid with a higher $^{18}O/^{16}O$ ratio than associated detrital dolomites. The wide range of high $\delta^{18}O$ values of the reconstructed fluid composition (+4–12‰) will be discussed in section 4.4).

Evidence for early dolomitization in both the Russøya and Petrovbreen members is consistent with studies of Tonian carbonates in Svalbard (Knoll & Swett, 1990) and other Neoproterozoic strata (Hood et al., 2011; Shuster et al., 2018; Tucker, 1982). Deep water dolomicrite firm or hardgrounds in non-glacial Cryogenian strata are interpreted as deep water authigenic deposits formed during sediment starvation (Wallace et al., 2019). The stratified diamictite above contains localized sulfate pseudomorphs and is laterally associated with sand wedges and brecciation (Fairchild and Hambrey, 1984; Fairchild, pers. comm.), interpreted as a syn-glacial depositional hiatus. If these Petrovbreen Member dolomicrites have a similar origin to other Cryogenian authigenic dolomicrites, then they originated under significantly different glacial environments than the ultimate subaerial exposure inferred by cross-cutting sand wedges (Fairchild & Hambrey, 1984).

4.3 Preservation of isotopic records in non-glacial facies

Despite evidence for early dolomite precipitation and coherence between clumped isotope temperatures and sedimentary indicators of climate, within the non-glacial dolomites clumped isotope temperatures vary from 48–77°C. The highest temperature samples are associated with consistent reconstructed fluid $\delta^{18}O$ values (Figure 3A), and this correspondence is consistent with fluid-buffered diagenetic alteration, wherein carbonates partially equilibrate to fluid $\delta^{18}O$ under elevated burial temperatures (Bergmann et al., 2018; Ryb & Eiler, 2018; Winkelstern & Lohmann, 2016). On account of this distinct fluid-buffered alteration signal, we have excluded the highest temperature non-glacial samples (≥73°C, n=3) from any paleoenvironmental analysis. Also excluded is two samples (one glacial, one preglacial; Table S1) with coarse dissolution and reprecipitation textures inconsistent with the textural preservation of surrounding strata. These samples are together referred to as the "altered dolomites" in subsequent discussion.

The remaining best-preserved samples from the Russøya Member have consistent clumped isotope temperatures (53±4°C, 1 sd n=7; Figure 5B). The traditional carbonate $\delta^{18}O$ thermometer (Horita, 2014) for these same samples also gives consistent, though lower, temperatures (37±4°C, 1 sd n=7) assuming modern seawater $\delta^{18}O$ values and no polar ice (-1.2‰ VSMOW, Lear et al., 2000; Cramer et al., 2011; see Bergmann et al., 2018a, 2018b and Henkes

et al., 2018 for discussion of paleomarine $\delta^{18}O$ values). The higher clumped isotope temperatures measured for all non-glacial facies correspond to higher reconstructed fluid $\delta^{18}O$ values than the assumed ice-free value of -1.2‰ VSMOW; non-glacial samples <50°C have fluid $\delta^{18}O$ values of +0.7 to +1.8‰ VSMOW (Figure 4). Higher fluid $\delta^{18}O$ values at elevated clumped isotope temperatures are consistent with rock-buffered dissolution and reprecipitation, cementation, or partial solid-state reordering increasing temperature with burial (Staudigel & Swart, 2019; Stolper et al., 2018). Given the association of evaporite pseudomorphs and stromatolites in the non-glacial facies association, it is also possible that fluid $\delta^{18}O$ values were higher from primary restriction and evaporative concentration in the depositional environment.

Uncertainty in the starting fluid composition complicates back-calculation of temperature from mineral $\delta^{18}O$, but assumption source fluid composition provides an estimate for diagenetic increase in clumped isotope temperature with rock-buffered alteration. If we take cross-cutting vein temperature of 122°C as a maximum burial temperature (see Discussion section 4.1), dolomites did not likely exceed the threshold for solid state reordering based on Arrhenius parameters of Lloyd et al. (2018). In this case, measured sample clumped isotope temperatures would instead represent a mixture between one component of carbonate equilibrated to depositional or early diagenetic conditions and another component equilibrated to deeper burial temperatures; under rock-buffered alteration, both components would have the same mineral $\delta^{18}O$ value. It would require at least a 16% contribution of burial-equilibrated dolomites to account for observed reconstructed $\delta^{18}O$ values if early dolomites precipitated from a -1.2‰ $\delta^{18}O$ VSMOW fluid as described above. Source waters with lower $\delta^{18}O$ values (e.g. Galili et al., 2019) would require proportionately greater burial alteration to explain the composition of the pre-glacial dolomites (Table 1).

Data treatment	Strata	$\delta^{18}O$ mineral (‰ VPDB)	Temp (°C)	Initial fluid $\delta^{18}O$ (‰ VSMOW)	% equilibrated to burial estimate (122°)
Raw data	Pre-glacial	-1.5/-2.2	48/53	**+1.8/+1.9**	0%
Raw data	Glacial	+7.9/+6.8	19/33	**+4.8/+6.9**	0%
Pre-glacial fluid $\delta^{18}O$ -1.2‰	Pre-glacial	-1.5/-2.2	**34/37**	-1.2	**22%/23%**
Pre-glacial fluid $\delta^{18}O$ -1.2‰	Glacial	+7.9/+6.8	**2/16**	**-0.1/+2.8**	22%/23%
Pre-glacial fluid $\delta^{18}O$ -5‰	Pre-glacial	-1.5/-2.2	**18/21**	-5	**39%/41%**
Pre-glacial fluid $\delta^{18}O$ -5‰	Glacial	+7.9/+6.8	**-16/-2**	**-6.3/-2.8**	39%/41%
15% equilibrated	*Pre-glacial*	*-1.5/-2.2*	***39/44***	***-0.1/0.2***	*15%*
15% equilibrated	*Glacial*	*+7.9/+6.8*	***8/23***	***+1.8/+4.5***	*15%*
30% equilibrated	Pre-glacial	-1.5/-2.2	**27/33**	**-2.7/-2.3**	30%
30% equilibrated	Glacial	+7.9/+6.8	**-6/10**	**-2.6/+0.9**	30%

Table 1: Summary of mineral $\delta^{18}O$, temperature, and initial source fluid $\delta^{18}O$ for pre- and syn-glacial dolomites. Data are presented for the lowest/mean sample temperatures associated with each climate state. Raw data are transformed via possible rock-buffered alteration trajectories based on hypothetical initial source fluid $\delta^{18}O$ values or the percent of dolomite equilibrated to peak burial estimate. For each data treatment, the pre-glacial percent equilibrated is used to estimate the initial fluid $\delta^{18}O$ values for glacial conditions. In each row of the transformed data, $\delta^{18}O$ mineral is held constant, and the treatment is used to calculate either the percent equilibrated (with initial fluid assumed) or initial fluid composition (with percent equilibrated assumed). Calculated values are in bold, and the preferred interpretation is italicized. In all treatments, the difference in minimum temperatures between pre-glacial and glacial states are similar to that of the raw data.

4.4 Stratigraphic changes in isotope geochemistry

If early dolomites have maintained a signal of their early clumped isotope composition through burial at Dracoisen, we predict that clumped isotope temperatures should covary with independent sedimentary records of climate. Indeed, the coldest reconstructed clumped isotope temperatures of Russøya Member non-glacial dolomite are 29°C warmer than the coldest temperatures recorded in the diamictite dolomicrite matrix. Taking the Russøya and Petrovbreen Member temperatures together, mean non-glacial temperatures are significantly warmer than glacial dolomicrites. The mean temperature of the non-glacial facies is between 16 and 36°C warmer than glacial dolomicrite by the Welch Two Sample t-test (n = 19, 95% confidence interval), excluding the altered dolomites (Section 4.3). This relationship is similar when all detrital clasts are binned with the non-glacial facies, giving a mean temperature between 12 and 29°C warmer than glacial dolomicrite (n = 31, 95% confidence interval; Figure 5A).

Changes to the local diagenetic environment and/or extent of dissolution and reprecipitation are not sufficient to explain the difference between the chemistry of the non-glacial facies and the overlying glacial dolomicrite facies. The lower temperatures, more positive fluid $\delta^{18}O$ values, and negative mineral $\delta^{13}C$ values of glacial diamictite matrix and soft sediment clasts are inconsistent with alteration trajectories of non-glacial facies. Rock-buffered alteration with burial or dolomitization by basinal brines would have the opposite trend with

higher reconstructed fluid $\delta^{18}O$ values at greater temperatures (e.g. Mangenot et al., 2018). Instead, the clumped isotope results of the Petrovbreen Member dolomicrite are consistent with early dolomite formation under different depositional or early diagenetic environments prior to deep burial. If both glacial and non-glacial facies experienced similar rock-buffered dissolution and reprecipitation (see Discussion section 4.3), then the early temperature and source fluid $\delta^{18}O$ values for glacial dolomicrite may have also been lower than measured in this clumped isotope analysis (33±9°C and +7±2‰, respectively; n = 12, 1 SD). For the lowest temperature dolomicrite and soft sediment samples (19°C and 21°C, respectively) and the hypothetical 15% contribution of dolomite equilibrated to burial temperatures (see Discussion section 4.3, Table 1), initial temperatures would have been +8°C and +10°C with a reconstructed fluid $\delta^{18}O$ values of +1.8‰ and +4.5‰, respectively (Figure 5B). The reconstructed fluid $\delta^{18}O$ values are more positive than modern seawater, albeit with less extreme values than initially calculated from the clumped isotope thermometer (+4.8‰ and +7.7‰). Higher levels of rock-buffered alteration would correspond to lower initial temperatures and lower source fluid $\delta^{18}O$ values (Table 1).

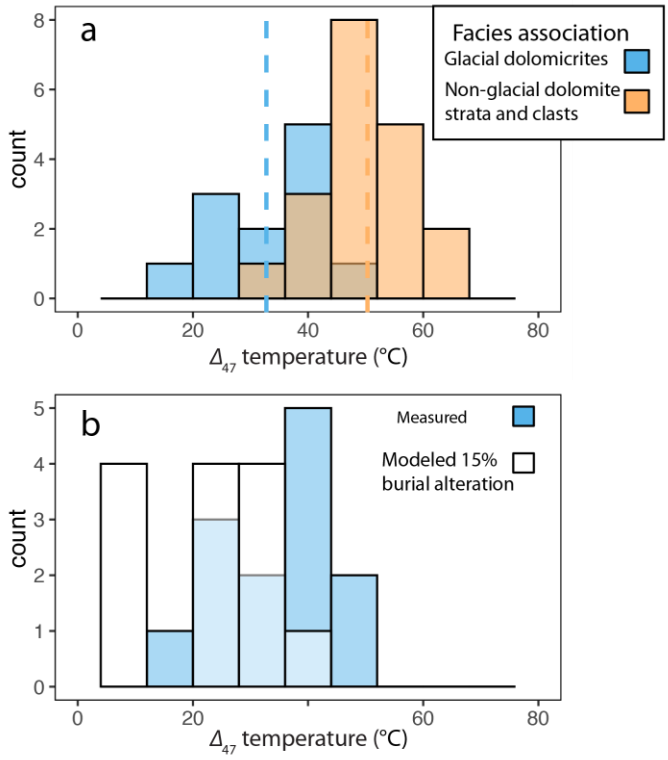

Figure 5: Histograms of clumped isotope data and reconstructions of initial conditions assuming partial rock-buffered alteration with burial. a) Histograms of glacial dolomicrite and aggregated pre-glacial dolomite and diamictite clast facies; vertical lines mark mean Δ_{47} temperatures. b) Glacial dolomicrite clumped isotope temperatures transformed with a modeled 15% contribution of dolomite equilibrated to burial temperatures, consistent with the interpreted alteration in pre-glacial carbonates (Table 1).

High $\delta^{18}O$ values for primary or early diagenetic glacial fluids are consistent with evaporative concentration, though the value cannot discern whether this evaporation relates to sequestration of precipitation in continental ice sheets (e.g. Raymo et al., 2018; Shackleton, 1967) or more local restriction (e.g. Gat, 1995; Horita, 2008). The association of these dolomites with diamictite does suggest at least some contribution from the former, however. Regardless of the mechanism for increase in fluid $\delta^{18}O$ values, results from the Petrovbreen Member dolomicrites suggest either net marine evaporation feeding ice sheet growth or local atmospheric exposure in this depositional environment to allow for continued evaporation. Other mechanisms for concentrating solutes in glacial environments like freeze-concentration (Staudigel et al.,

2018) cannot explain the observed trends here, as freeze concentration is associated with lower fluid $\delta^{18}O$ values (Horita, 2008).

4.5 Implications for Neoproterozoic glacial episodes

Evidence for evaporation coincident with the deposition of Petrovbreen Member cold water carbonate beds constrains depositional and early diagenetic conditions at points within this glacial episode. Relatively high fluid $\delta^{18}O$ values in glacial carbonates compared to underlying non-glacial strata, is most consistent with intervals of moderate glaciation with an active hydrologic cycle, rather than the permanent ice shell predicted by more severe hypotheses for Snowball Earth. Relative changes in temperature between non-glacial and glacial facies also inform reconstructions of the magnitude of climate perturbation represented by these strata. The offset in minimum temperatures (29°C) between non-glacial and glacial low latitude carbonates is more severe than reconstructed for Phanerozoic glaciations (Finnegan et al., 2011; Grossman et al., 2008; Raymo et al., 2018), but more moderate than predicted for the most severe hypotheses of Snowball glaciation (Abbot et al., 2013; Hoffman et al., 2017 and references therein).

5 Conclusions

The Neoproterozoic Elbobreen Formation of NE Svalbard contains carbonate-rich facies preceding and coincident with the first Cryogenian Snowball Earth episode. These carbonates preserve shifts in $\delta^{18}O$ composition and Δ_{47} temperature records alongside sedimentological evidence of environmental change. When combined in stratigraphic and petrographic context, these geochemical records indicate that primary to early diagenetic conditions have been partially preserved in these Neoproterozoic carbonates. Whereas calcite clumped isotope temperatures have been partially altered (92±5°C, 1 sd) through solid state reordering during deep burial, the more recalcitrant dolomites retain informative clumped isotope temperature relationships. Dolomite clumped isotope temperatures are warmer than expected for surface depositional environments, but relative temperatures and reconstructed source water $\delta^{18}O$ values co-vary with independent sedimentological evidence for climate change. Minimum temperatures for glacial facies are 29°C colder than non-glacial facies, and detrital dolomitic clasts from the glacial diamictites retain temperatures and mineral $\delta^{18}O$ values consistent with diverse glacial and non-glacial sources. Source waters for glacial facies also have higher $\delta^{18}O$ values than non-glacial facies, with minimum reconstructed $\delta^{18}O$ fluid values >3‰ higher between these facies. Together, results indicate that there were both detrital and autochthonous sources of dolomite in these glacial environments. Temperature changes and higher fluid $\delta^{18}O$ values are consistent with moderate glacial environments with an active hydrological cycle, indicating some combination of evaporative concentration of surface waters or growth of ice sheets with evaporation from of a marine reservoir. Results are not consistent with interpretations of ice sheets formed by freeze concentration and persistent shutdown of the hydrological cycle expected in the most severe models for Snowball Earth episodes. Further constraints on conditions surrounding panglacial climate episodes may be feasible through judicious application of carbonate clumped isotope thermometry in other well-preserved Neoproterozoic strata.

Data

All data used in this study are available in this article and its online supplemental materials. Raw data from carbonate clumped isotope analysis are submitted for review as supplemental materials and will be submitted to the EARTHCHEM Database by acceptance.

Acknowledgments

We thank A. Knoll for his insights into Svalbard carbonate stratigraphy and discussion of promising field localities. Field work in 2014 was conducted by K. Bergmann and J. Creveling and was supported by the Harvard Society of Fellows and the Milton Fund at Harvard University; J. Cooper assisted in collecting and documenting samples. Discussions with I. Fairchild and his contribution of additional samples improved this study. G. Halverson, J. Strauss, and N. Tosca further informed our work through their helpful discussions. We would also like to thank Magali Bonifacie, Lou Derry and Bergmann lab members M. Cantine, J. Wilcots, and S. Goldberg for comments and suggestions on earlier drafts of this manuscript. TJM was supported by an Agouron Institute Postdoctoral Fellowship. K. Bergmann acknowledges support for laboratory expenses from the MIT Node of the NASA Astrobiology Institute, NASA Exobiology grant 80NSSC19K0464, and the MIT Wade Fund and the Packard Foundation. We have no conflicts of interest with respect to the results of this paper.

References

Abbot, D. S., Voigt, A., & Koll, D. (2011). The Jormungand global climate state and implications for Neoproterozoic glaciations. *Journal of Geophysical Research*, *116*(D18), D18103. https://doi.org/10.1029/2011JD015927

Abbot, D. S., Voigt, A., Li, D., Hir, G. Le, Pierrehumbert, R. T., Branson, M., et al. (2013). Robust elements of Snowball Earth atmospheric circulation and oases for life. *Journal of Geophysical Research: Atmospheres*, *118*(12), 6017–6027. https://doi.org/10.1002/jgrd.50540

Bergmann, K. D., Al Balushi, S. A. K., Mackey, T. J., Grotzinger, J. P., & Eiler, J. M. (2018). A 600-Million-Year Carbonate Clumped-Isotope Record from the Sultanate of Oman. *Journal of Sedimentary Research*, *88*(8), 960–979. https://doi.org/10.2110/jsr.2018.51

Bergmann, K. D., Finnegan, S., Creel, R., Eiler, J. M., Hughes, N. C., Popov, L. E., & Fischer, W. W. (2018). A paired apatite and calcite clumped isotope thermometry approach to estimating Cambro-Ordovician seawater temperatures and isotopic composition. *Geochimica et Cosmochimica Acta*, *224*, 18–41. https://doi.org/10.1016/J.GCA.2017.11.015

Bergström, S. M. (1980). Conodonts as paleotemperature tools in Ordovician rocks of the Caledonides and adjacent areas in Scandinavia and the British Isles. *Geologiska Foreningens i Stockholm Forhandlingar*, *102*(4), 377–392. https://doi.org/10.1103/PhysRevLett.101.105501

Bernasconi, S. M., Müller, I. A., Bergmann, K. D., Breitenbach, S. F. M., Fernandez, A., Hodell, D. A., et al. (2018). Reducing Uncertainties in Carbonate Clumped Isotope Analysis Through Consistent Carbonate-Based Standardization. *Geochemistry, Geophysics, Geosystems*. https://doi.org/10.1029/2017GC007385

739 Bird, M. I., Chivas, A. R., Radnell, C. J., & Burton, H. R. (1991). Sedimentological and stable-
740 isotope evolution of lakes in the Vestfold Hills, Antarctica. *Palaeogeography,*
741 *Palaeoclimatology, Palaeoecology, 84*(1–4), 109–130. https://doi.org/10.1016/0031-
742 0182(91)90039-T

743 Brenchley, P. J., Marshall, J. D., Carden, G. A. F., Robertson, D. B. R., Long, D. G. F., Meidla,
744 T., et al. (1994). Bathymetric and isotopic evidence for a short-lived Late Ordovician
745 glaciation in a greenhouse period. *Geology*, *22*(4), 295–298. https://doi.org/10.1130/0091-
746 7613(1994)022<0295:BAIEFA>2.3.CO;2

747 Cohen, P. A., & Riedman, L. A. (2018). It's a protist-eat-protist world: recalcitrance, predation,
748 and evolution in the Tonian–Cryogenian ocean. *Emerging Topics in Life Sciences*, *2*(2),
749 173–180. https://doi.org/10.1042/ETLS20170145

750 Cramer, B. S., Miller, K. G., Barrett, P. J., & Wright, J. D. (2011). Late Cretaceous–Neogene
751 trends in deep ocean temperature and continental ice volume: Reconciling records of
752 benthic foraminiferal geochemistry (δ^{18}O and Mg/Ca) with sea level history. *Journal of*
753 *Geophysical Research*, *116*(C12), C12023. https://doi.org/10.1029/2011JC007255

754 Daëron, M., Blamart, D., Peral, M., & Affek, H. P. (2016). Absolute isotopic abundance ratios
755 and the accuracy of Δ47 measurements. *Chemical Geology*, *442*, 83–96.
756 https://doi.org/10.1016/J.CHEMGEO.2016.08.014

757 Defliese, W. F., Hren, M. T., & Lohmann, K. C. (2015). Compositional and temperature effects
758 of phosphoric acid fractionation on δ47 analysis and implications for discrepant
759 calibrations. *Chemical Geology*, *396*, 51–60. https://doi.org/10.1016/j.chemgeo.2014.12.018

760 Dickson, J. A. D., & Coleman, M. L. (1980). Changes in Carbon and Oxygen Isotope
761 Composition during Limestone Diagenesis. *Sedimentology*, *27*, 107–118.
762 https://doi.org/10.1002/9781444304510.ch21

763 Dörr, N., Lisker, F., Clift, P. D., Carter, A., Gee, D. G., Tebenkov, A. M., & Spiegel, C. (2012).
764 Late Mesozoic-Cenozoic exhumation history of northern Svalbard and its regional
765 significance: Constraints from apatite fission track analysis. *Tectonophysics*, *514–517*, 81–
766 92. https://doi.org/10.1016/j.tecto.2011.10.007

767 Dörr, Nina, Lisker, F., Piepjohn, K., & Spiegel, C. (2019). Cenozoic development of northern
768 Svalbard based on thermochronological data. *Terra Nova*, *31*(3), 306–315.
769 https://doi.org/10.1111/ter.12402

770 Eiler, J. M. (2007). "Clumped-isotope" geochemistry-The study of naturally-occurring, multiply-
771 substituted isotopologues. *Earth and Planetary Science Letters*, *262*(3–4), 309–327.
772 https://doi.org/10.1016/j.epsl.2007.08.020

773 Epstein, A. G., Epstein, J. B., & Harris, L. D. (1977). Conodont color alteration - an index to
774 organic metamorphism. *USGS Professional Paper*, *995*, 27pp. https://doi.org/10.1130/0016-
775 7606(1987)99<471:CCATAA>2.0.CO;2

776 Fairchild, I J, Hambrey, M. J., Spiro, B., & Jefferson, T. H. (1989). Late Proterozoic glacial
777 carbonates in northeast Spitsbergen: new insights into the carbonate–tillite association.
778 *Geological Magazine*, *126*(05), 469–490.

779 Fairchild, Ian J., & Hambrey, M. J. (1984). The Vendian succession of northeastern Spitsbergen:

780 Petrogenesis of a dolomite-tillite association. *Precambrian Research*, *26*(2), 111–167.
781 https://doi.org/10.1016/0301-9268(84)90042-1

782 Fairchild, Ian J., Bradby, L., & Spiro, B. (2004). Reactive carbonate in glacial systems: a
783 preliminary synthesis of its creation, dissolution and reincarnation. In M. Deynoux, J. M. G.
784 Miller, & E. W. Domack (Eds.), *Earth's Glacial Record* (pp. 176–192). Cambridge
785 University Press.

786 Fairchild, Ian J., Spencer, A. M., Ali, D. O., Anderson, R. P., Anderton, R., Boomer, I., et al.
787 (2017). Tonian-Cryogenian boundary sections of Argyll, Scotland. *Precambrian Research*.
788 https://doi.org/10.1016/J.PRECAMRES.2017.09.020

789 Fairchild, Ian J. (1983). Effects of glacial transport and neomorphism on Precambrian dolomite
790 crystal sizes. *Nature*, *304*(August), 714–716.

791 Fairchild, Ian J, Bonnand, P., Davies, T., Fleming, E. J., Grassineau, N., Halverson, G. P., et al.
792 (2016). The Late Cryogenian Warm Interval , NE Svalbard : Chemostratigraphy and
793 genesis, *281*, 128–154.

794 Fernandez, A., Muller, I. A., Rodriguez-Sanz, L., Van Dijk, J., Looser, N., & Bernasconi, S. M.
795 (2017). A Reassessment of the Precision of Carbonate Clumped Isotope Measurements:
796 Implications for Calibrations and Paleoclimate Reconstructions. *Geochemistry, Geophysics,*
797 *Geosystems*, *18*, 4375–4386. https://doi.org/10.1002/2017GC007106

798 Ferry, J. M., Passey, B. H., Vasconcelos, C., & Eiler, J. M. (2011). Formation of dolomite at 40–
799 80 °C in the Latemar carbonate buildup, Dolomites, Italy, from clumped isotope
800 thermometry. *Geology*, *39*(6), 571–574. https://doi.org/10.1130/G31845.1

801 Finnegan, S., Bergmann, K., Eiler, J. M., Jones, D. S., Fike, D. A., Eisenman, I., et al. (2011).
802 The magnitude and duration of Late Ordovician-Early Silurian glaciation. *Science (New*
803 *York, N.Y.)*, *331*(6019), 903–6. https://doi.org/10.1126/science.1200803

804 Frank, T. D., Gui, Z., & ANDRILL SMS Science Team. (2010). Cryogenic origin for brine in
805 the subsurface of southern McMurdo Sound, Antarctica. *Geology*, *38*(7), 587–590.
806 https://doi.org/10.1130/G30849.1

807 Galili, N., Shemesh, A., Yam, R., Brailovsky, I., Sela-adler, M., Schuster, E. M., et al. (2019).
808 The geological history of seawater oxygen isotopes from marine iron oxides. *Science*,
809 *473*(August), 469–473.

810 Gasser, D. (2014). The Caledonides of Greenland, Svalbard and other Arctic areas: status of
811 research and open questions. In F. Corfu, D. Gasser, & D. M. Chew (Eds.), *New*
812 *Perspectives on the Caledonides of Scandinavia and Related Areas* (pp. 93–129).
813 Geological Society, London, Special Publications. https://doi.org/10.1144/SP390.17

814 Gat, J. R. (1995). Fresh and ready... In A. Lerman, D. M. Imboden, & J. R. Gat (Eds.), *Physics*
815 *and Chemistry of Lakes*. New York: Springer-Verlag.

816 Grossman, E. L., Yancey, T. E., Jones, T. E., Bruckschen, P., Chuvashov, B., Mazzullo, S. J., &
817 Mii, H.-S. (2008). Glaciation, aridification, and carbon sequestration in the Permo-
818 Carboniferous: The isotopic record from low latitudes.
819 https://doi.org/10.1016/j.palaeo.2008.03.053

820 Halverson, G. P., Maloof, A. C., & Hoffman, P. F. (2004). The Marinoan glaciation (

Neoproterozoic) in northeast Svalbard, 297–324. https://doi.org/10.1111/j.1365-2117.2004.00234.x

Halverson, G. P., Kunzmann, M., Strauss, J. V., & Maloof, A. C. (2018). The Tonian-Cryogenian transition in Northeastern Svalbard. *Precambrian Research*, *319*, 79–95. https://doi.org/10.1016/J.PRECAMRES.2017.12.010

Hambrey, M. J. (1982). Late Precambrian diamictites of northeastern Svalbard. *Geological Magazine*, *119*(06), 527. https://doi.org/10.1017/S0016756800027035

Harland, W. B., Wallis, R. H., & Gayer, R. A. (1966). A Revision of the Lower Hecla Hoek Succession in Central North Spitsbergen and Correlation Elsewhere. *Geological Magazine*, *103*(01), 70. https://doi.org/10.1017/S0016756800050433

Henkes, G. A., Passey, B. H., Grossman, E. L., Shenton, B. J., Pérez-Huerta, A., & Yancey, T. E. (2014). Temperature limits for preservation of primary calcite clumped isotope paleotemperatures. *Geochimica et Cosmochimica Acta*, *139*, 362–382. https://doi.org/10.1016/J.GCA.2014.04.040

Henkes, G. A., Passey, B. H., Grossman, E. L., Shenton, B. J., Yancey, T. E., & Pérez-Huerta, A. (2018). Temperature evolution and the oxygen isotope composition of Phanerozoic oceans from carbonate clumped isotope thermometry. *Earth and Planetary Science Letters*, *490*, 40–50. https://doi.org/10.1016/J.EPSL.2018.02.001

Hoffman, P. F., Kaufman, A. J., Halverson, G. P., & Schrag, D. P. (1998). A neoproterozoic snowball earth. *Science (New York, N.Y.)*, *281*(5381), 1342–6. https://doi.org/10.1126/SCIENCE.281.5381.1342

Hoffman, P. F., Halverson, G. P., Domack, E. W., Maloof, A. C., Swanson-hysell, N. L., & Cox, G. M. (2012). Cryogenian glaciations on the southern tropical paleomargin of Laurentia (NE Svalbard and East Greenland), and a primary origin for the upper Russøya (Islay) carbon isotope excursion. *Precambrian Research*, *206–207*, 137–158. https://doi.org/10.1016/j.precamres.2012.02.018

Hoffman, P. F., Abbot, D. S., Ashkenazy, Y., Benn, D. I., Brocks, J. J., Cohen, P. A., et al. (2017). Snowball Earth climate dynamics and Cryogenian. *Science Advances*, *3*(e1600983).

Hood, A. V. S., Wallace, M. W., & Drysdale, R. N. (2011). Neoproterozoic aragonite-dolomite seas? Widespread marine dolomite precipitation in Cryogenian reef complexes. *Geology*, *39*(9), 871–874. https://doi.org/10.1130/G32119.1

Horita, J. (2008). Isotopic Evolution of Saline Lakes in the Low-Latitude and Polar Regions. *Aquatic Geochemistry*, *15*(1–2), 43–69. https://doi.org/10.1007/s10498-008-9050-3

Horita, J. (2014). ScienceDirect Oxygen and carbon isotope fractionation in the system dolomite – water – CO 2 to elevated temperatures, *129*, 111–124. https://doi.org/10.1016/j.gca.2013.12.027

Huntington, K. W., Budd, D. A., Wernicke, B. P., & Eiler, J. M. (2011). Use of Clumped-Isotope Thermometry To Constrain the Crystallization Temperature of Diagenetic Calcite. *Journal of Sedimentary Research*, *81*(9), 656–669. https://doi.org/10.2110/jsr.2011.51

John, C. M., & Bowen, D. (2016). Community software for challenging isotope analysis: First applications of 'Easotope' to clumped isotopes. *Rapid Communications in Mass*

Spectrometry, *30*(21), 2285–2300. https://doi.org/10.1002/rcm.7720

Kim, S.-T., & O'Neil, J. R. (1997). Equilibrium and nonequilibrium oxygen isotope effects in synthetic carbonates. *Geochimica et Cosmochimica Acta*, *61*(16), 3461–3475. https://doi.org/10.1016/S0016-7037(97)00169-5

Kirschvink, J. L. (1992). Late Proterozoic Low-Latitude Global Glaciation: the Snowball Earth. In *Geological Evolution of the Proterozoic Earth* (pp. 51–52). Retrieved from https://authors.library.caltech.edu/36446/1/Kirschvink_1992p51.pdf

Knoll, A. H., & Calder, S. (1983). Microbiotas of the Late Precambrian Rysso Formation, Nordaustlandet, Svalbard. *Palaeontology*, *26*(3), 467–496. Retrieved from https://cdn.palass.org/publications/palaeontology/volume_26/pdf/vol26_part3_pp467-496.pdf

Knoll, A. H., & Swett, K. (1990). Carbonate deposition during the late Proterozoic Era: An example from Spitsbergen. *American Journal of Science*, *290A*, 104–132.

Lea, D. W., Pak, D. K., & Spero, H. J. (2000). Climate Impact of Late Quaternary Equatorial Pacific Sea Surface Temperature Variations. *Science*, *289*(5485), 1719–1724. https://doi.org/10.1126/science.289.5485.1719

Lear, C. H., Elderfield, H., & Wilson, P. A. (2000). Cenozoic deep-sea temperatures and global ice volumes from Mg/Ca in benthic foraminiferal calcite. *Science*, *287*(5451), 269–272. https://doi.org/10.1126/science.287.5451.269

Lee, C., Love, G. D., Hopkins, M. J., Kröger, B., Franeck, F., & Finnegan, S. (2019). Lipid biomarker and stable isotopic profiles through Early-Middle Ordovician carbonates from Spitsbergen, Norway. *Organic Geochemistry*, *131*, 5–18. https://doi.org/10.1016/j.orggeochem.2019.02.008

Lloyd, M. K., Ryb, U., & Eiler, J. M. (2018). Experimental calibration of clumped isotope reodering in dolomite. *Geochimica et Cosmochimica Acta*. https://doi.org/10.1016/J.GCA.2018.08.036

Lohmann, K. C. (1988). Geochemical Patterns of Meteoric Diagenetic Systems and Their Application to Studies of Paleokarst. In N. P. James & P. W. Choquette (Eds.), *Paleokarst* (pp. 58–80). New York, NY: Springer New York. https://doi.org/10.1007/978-1-4612-3748-8_3

Macdonald, F. A., Schmitz, M. D., Crowley, J. L., Roots, C. F., Jones, D. S., Maloof, A. C., et al. (2010). Calibrating the Cryogenian. *Science*, *327*(5970), 1241–1243. https://doi.org/10.1126/science.1183325

MacLennan, S., Park, Y., Swanson-Hysell, N., Maloof, A., Schoene, B., Gebreslassie, M., et al. (2018). The arc of the Snowball: U-Pb dates constrain the Islay anomaly and the initiation of the Sturtian glaciation. *Geology*, *46*(6), 539–542. https://doi.org/10.1130/G40171.1

Maloof, A. C., Halverson, G. P., Kirschvink, J. L., Schrag, D. P., Weiss, B. P., & Hoffman, P. F. (2006). Combined paleomagnetic, isotopic, and stratigraphic evidence for true polar wander from the Neoproterozoic Akademikerbreen Group, Svalbard, Norway. *Geological Society of America Bulletin*, *118*(9–10), 1099–1124. https://doi.org/10.1130/B25892.1

Mangenot, X., Gasparrini, M., Rouchon, V., & Bonifacie, M. (2018). Basin-scale thermal and

fluid flow histories revealed by carbonate clumped isotopes (Δ_{47}) - Middle Jurassic carbonates of the Paris Basin depocentre. *Sedimentology*, *65*(1), 123–150. https://doi.org/10.1111/sed.12427

Montañez, I. P., & Poulsen, C. J. (2013). The Late Paleozoic Ice Age: An Evolving Paradigm. *Annual Review of Earth and Planetary Sciences*, *41*(1), 629–656. https://doi.org/10.1146/annurev.earth.031208.100118

Müller, I. A., Violay, M. E. S., Storck, J. C., Fernandez, A., van Dijk, J., Madonna, C., & Bernasconi, S. M. (2017). Clumped isotope fractionation during phosphoric acid digestion of carbonates at 70 °C. *Chemical Geology*, *449*, 1–14. https://doi.org/10.1016/j.chemgeo.2016.11.030

Partin, C. A., & Sadler, P. M. (2016). Slow net sediment accumulation sets snowball Earth apart from all younger glacial episodes. *Geology*, *44*(12), 1019–1022. https://doi.org/10.1130/G38350.1

Passey, B. H., & Henkes, G. A. (2012). Carbonate clumped isotope bond reordering and geospeedometry. *Earth and Planetary Science Letters*, *351–352*, 223–236. https://doi.org/10.1016/j.epsl.2012.07.021

Raymo, M. E., Kozdon, R., Evans, D., Lisiecki, L., & Ford, H. L. (2018). The accuracy of mid-Pliocene δ18O-based ice volume and sea level reconstructions. *Earth-Science Reviews*, *177*, 291–302. https://doi.org/10.1016/J.EARSCIREV.2017.11.022

Rooney, A. D., Strauss, J. V., Brandon, A. D., & Macdonald, F. A. (2015). A Cryogenian chronology: Two long-lasting synchronous Neoproterozoic glaciations. *Geology*, *43*(5), 459–462. https://doi.org/10.1130/G36511.1

Ryb, U., & Eiler, J. M. (2018). Oxygen isotope composition of the Phanerozoic ocean and a possible solution to the dolomite problem. *Proceedings of the National Academy of Sciences of the United States of America*, *115*(26), 6602–6607. https://doi.org/10.1073/pnas.1719681115

Schauer, A. J., Kelson, J., Saenger, C., & Huntington, K. W. (2016). Choice of ^{17}O correction affects clumped isotope (Δ_{47}) values of CO_2 measured with mass spectrometry. *Rapid Communications in Mass Spectrometry*, *30*(24), 2607–2616. https://doi.org/10.1002/rcm.7743

Shackleton, N. (1967). Oxygen Isotope Analyses and Pleistocene Temperatures Re-assessed. *Nature*, *215*(5096), 15–17. https://doi.org/10.1038/215015a0

Shuster, A. M., Wallace, M. W., van Smeerdijk Hood, A., & Jiang, G. (2018). The Tonian Beck Spring Dolomite: Marine dolomitization in a shallow, anoxic sea. *Sedimentary Geology*, *368*, 83–104. https://doi.org/10.1016/J.SEDGEO.2018.03.003

Spence, G. H., Le Heron, D. P., & Fairchild, I. J. (2016). Sedimentological perspectives on climatic, atmospheric and environmental change in the Neoproterozoic Era. *Sedimentology*, *63*(2), 253–306. https://doi.org/10.1111/sed.12261

Spencer, A. M. (1971). Late Pre-cambrian Glaciation In Scotland. *Geological Society Memoir*, *6*(1), 5–102. https://doi.org/10.1144/GSL.MEM.1971.006.01.02

Staudigel, P. T., & Swart, P. K. (2019). A diagenetic origin for isotopic variability of sediments

deposited on the margin of Great Bahama Bank, insights from clumped isotopes. *Geochimica et Cosmochimica Acta*, *258*, 97–119. https://doi.org/10.1016/j.gca.2019.05.002

Staudigel, P. T., Murray, S., Dunham, D. P., Frank, T. D., Fielding, C. R., & Swart, P. K. (2018). Cryogenic brines as diagenetic fluids: Reconstructing the diagenetic history of the Victoria Land Basin using clumped isotopes. *Geochimica et Cosmochimica Acta*, *224*, 154–170. https://doi.org/10.1016/J.GCA.2018.01.002

Stolper, D. A., & Eiler, J. M. (2015). The kinetics of solid-state isotope-exchange reactions for clumped isotopes: A study of inorganic calcites and apatites from natural and experimental samples. *American Journal of Science*, *315*(5), 363–411. https://doi.org/10.2475/05.2015.01

Stolper, D. A., Eiler, J. M., & Higgins, J. A. (2018). Modeling the effects of diagenesis on carbonate clumped-isotope values in deep- and shallow-water settings. *Geochimica et Cosmochimica Acta*, *227*, 264–291. https://doi.org/10.1016/J.GCA.2018.01.037

Tucker, M. E. (1982). Precambrian dolomites: Petrographic and isotopic evidence that they differ from Phanerozoic dolomites. *Geology*, *10*(1), 7. https://doi.org/10.1130/0091-7613(1982)10<7:PDPAIE>2.0.CO;2

Urey, H. C. (1948). *Oxygen Isotopes in Nature and in the Laboratory*. *Science* (Vol. 108). Retrieved from http://web.gps.caltech.edu/~tsai/files/GreatPapers/Urey_1948.pdf

Wallace, M. W., Hood, A. v. S., Fayle, J., Hordern, E. S., & O'Hare, T. F. (2019). Neoproterozoic marine dolomite hardgrounds and their relationship to cap dolomites. *Precambrian Research*, *328*, 269–286. https://doi.org/10.1016/J.PRECAMRES.2019.04.026

Winkelstern, I. Z., & Lohmann, K. C. (2016). Shallow burial alteration of dolomite and limestone clumped isotope geochemistry. *Geology*, *44*(6), 467–470. https://doi.org/10.1130/G37809.1

Figure 1: Stratigraphy of the latest Tonian (Dartboard Dolomite and Russøya members) and earliest Cryogenian (Petrovbreen Member) at the Dracoisen Nunatak, NE Svalbard. **a**) Stratigraphic column highlighting transitions among the dominant carbonate mineralogies. The scale of the Petrovbreen Member is extended to display diamictite distribution. **b**) Composite of $\delta^{13}C$ values and **c**) Mineral $\delta^{18}O$ value through stratigraphic section. **d**) Clumped isotope temperatures and 95% CL error for a subset of these samples.

Figure 2: Petrographic textures of the Dracoisen section dolomites; where images are paired, left is a scanned polished sample and right is thin section photomicrograph. **a–c**) Glacial carbonates of the Petrovbreen Member consisting of **a**) homogeneous dolomicrite matrix, **b**) discrete soft sediment clasts in diamictite, **c**) detrital clasts and matrix consisting of <1 mm detrital clasts. **d** and **e**) non-glacial carbonates of the peritidal Dartboard Dolomite Member of the Akademikerbreen Formation and overlying Elbobreen Formation Russøya Member. Russøya Member dolomite facies pictured here include stromatolites with a clotted microtexture, evaporite pseudomorphs partially replaced by dolomite and silica (here cross-polarized to highlight twinning after gypsum), and homogeneous dolomicrospar rhombs in wedged thin section. Mean crystal sizes indicate range in mean sizes for analyzed samples, and isotope data

present the mean mineral $\delta^{18}O$ values and clumped-isotope temperatures ±1 standard deviation to describe the population analyzed, and the range of mean clumped-isotope temperatures.

Figure 3: Summary of standard and clumped isotope values with petrographic observation. **a**) Measured clumped-isotope temperature for carbonate samples versus the reconstructed fluid $\delta^{18}O$ values. 95% CL error bars are diagonal due dependence of reconstructed fluid $\delta^{18}O$ values on measurement temperature. RB/SSR line denotes reconstructed fluid composition for dolomites (Horita, 2014) under purely rock-buffered alteration or solid state reordering, given a starting fluid composition of -1.2‰. **b**) Measured clumped isotope temperature versus mineral $\delta^{13}C$. **c**) Mean crystal size varies with clumped isotope temperatures. Mean crystal size of diamictite clasts is consistent with the source stratigraphy inferred from reconstructed $\delta^{18}O$ fluid values and clumped-isotope temperatures. Calcite versus dolomite mineralogy does not appear to correspond to a significant difference in mean crystal size, despite elevated calcite temperatures interpreted as evidence of solid-state reordering. Crystal sizes <5 μm are approximate due to thickness of petrographic thin sections.

Figure 4: Cross plot of carbonate $\delta^{13}C$ and $\delta^{18}O$ values from the Tonian–Cryogenian in NE Svalbard. Pre-glacial carbonates from Halverson et al. (2005; 2007) sample the Russøya Member regionally as well as the underlying Akademikerbreen Formation. Glacial Petrovbreen Member carbonates sampled here are exclusively dolomitic. Diamictite clasts span the full range of $\delta^{13}C$ values in the underlying stratigraphy, but are generally more enriched in ^{18}O. Petrovbreen Member carbonate isotopic values are consistent with both a detrital carbonate source and a glacial source with higher $\delta^{18}O$ values, with soft sediment clasts making up the end member with the highest $\delta^{18}O$ values.

Figure 5: Histograms of clumped isotope data and reconstructions of initial conditions assuming partial rock-buffered alteration with burial. **a**) Histograms of glacial dolomicrite and aggregated pre-glacial dolomite and diamictite clast facies; vertical lines mark mean Δ_{47} temperatures. **b**) Glacial dolomicrite clumped isotope temperatures transformed with a modeled 15% contribution of dolomite equilibrated to burial temperatures, consistent with the interpreted alteration in pre-glacial carbonates (**Table 1**).

Table 1: Summary of mineral $\delta^{18}O$, temperature, and initial source fluid $\delta^{18}O$ for pre- and syn-glacial dolomites. Data are presented for the lowest/mean sample temperatures associated with each climate state. Raw data are transformed via possible rock-buffered alteration trajectories based on hypothetical initial source fluid $\delta^{18}O$ values or the percent of dolomite equilibrated to peak burial estimate. For each data treatment, the pre-glacial percent equilibrated is used to estimate the initial fluid $\delta^{18}O$ values for glacial conditions. In each row of the transformed data, $\delta^{18}O$ mineral is held constant, and the treatment is used to calculate either the percent equilibrated (with initial fluid assumed) or initial fluid composition (with percent equilibrated assumed). Calculated values are in bold, and the preferred interpretation is italicized. In all treatments, the difference in minimum temperatures between pre-glacial and glacial states are similar to that of the raw data.